RSC Advances

PAPER

View Article Online
View Journal | View Issue

Cite this: *RSC Adv.*, 2023, **13**, 5473

Supramolecular porphyrin as an improved photocatalyst for chloroform decomposition

J. M. S. Lopes, *[ad] A. A. Batista, [b] P. T. Araujo*[c] and N. M. Barbosa Neto *[d]

Received 4th December 2022
Accepted 2nd February 2023

DOI: 10.1039/d2ra07720e

rsc.li/rsc-advances

In this work, the outlying decoration of the free-base *meso*-(4-tetra) pyridyl porphyrin (H_2TPyP) with the **RuCl(dppb)(5,5′-Me-bipy)** ruthenium complex (here named **Supra-H_2TPyP**) is observed as an improved molecular photocatalyst for dye-mediated chloroform ($CHCl_3$) decomposition *via* one-photon absorption operating in the visible spectral range (532 nm and 645 nm). **Supra-H_2TPyP** offers a better option for $CHCl_3$ photodecomposition when compared to the same process mediated by pristine H_2TPyP, which requires either excited-state- or UV absorption. The chloroform photodecomposition rates for **Supra-H_2TPyP** as well as its excitation mechanisms are explored as a function of distinct laser irradiation conditions.

1. Introduction

Chlorine-derived disinfectants like sodium hypochlorite, chloramine, and chlorine dioxide are important structures for the treatment of drinking water and swimming pools.[1–5] Despite their good effectiveness in killing pathogenic microorganisms, unfortunately, when these substances interact with natural organic matter (*e.g.*, urine, sweat, and saliva) non-negligible amounts of undesired byproducts can be generated. Among them, chloroform ($CHCl_3$) brings significant concerns to health due to its cytotoxic effects.[1,6–8] In recent years, two major efforts have been conducted to deal with this problem: (1) the development of novel molecular sensors to detect chloroform in water,[9–11] and (2) the creation of methodologies to decompose this molecule in solution. Concerning the effort (2), although the biotechnological[12,13] and the pulsed-corona-discharges-assisted[14] approaches have been lately tested, the dye-catalyzed photochemical-based approaches stand as low-cost, non-invasive, selective, and controllable alternatives.[15–20]

The excited-state dynamics exhibited by porphyrins[21–25] set them as versatile molecular photocatalysts[15,26–29] that have been explored in fields like dye-sensitized solar cells,[30–33] photomedicine,[34–36] and artificial photosynthesis.[37–39] In the last decades, these macrocycle molecules have been explored as photocatalysts for dye-mediated decomposition of chloroform ($CHCl_3$) under one-photon absorption (OPA) and/or excited-state absorption (ESA).[15,16] Differently from visible light OPA, ultra-violet OPA (λ_{exc} = 266 nm) accesses the porphyrin's photooxidative excited states enabling the decomposition of $CHCl_3$ through an oxi-reduction reaction, which yields hydrochloric acid (HCl) and other products.[15] More recently, ESA[16] became an alternative approach to employ visible radiation for $CHCl_3$ photodecomposition.

The tunning of the excitation energy threshold for photo-oxidation could allow the photo-reaction to occur at lower-(higher-) energy OPA (ESA) but is still poorly explored. The synthesis of novel porphyrinic structures could facilitate such energy threshold controllability. Examples of synthetic approaches are: (1) the inner and outer macrocycle decoration;[21,40,41] (2) oligomer formation involving one or more types of porphyrins;[38,42–44] and (3) supramolecular porphyrin structures.[26,45–51] The attachment of metallic complexes (*e.g.*, ruthenium-, rhenium- and iridium-derived) at the outer positions of porphyrins generates supramolecular structures that offer novel excited states for achieving the photo-reaction threshold while keeping original states from both the pristine porphyrin and the complexes.[46,48,49,52–56]

In this work, a supramolecular structure originated from the attachment of the **RuCl(dppb)(5,5′-Me-bipy)** ruthenium complex at each (4-pyridyl) site of the *meso*-tetra(4-pyridyl) free-base porphyrin (**H_2TPyP**) is used as a molecular photocatalyst for $CHCl_3$ decomposition, allowing the reaction to occur *via* visible-light OPA. The influence of the excitation wavelength and mechanisms on the photo-reaction rates is also explored.

[a]*Department of Physics, Federal University of Roraima, Boa Vista, RR, Brazil. E-mail: lopesjefferson01@yahoo.com.br*

[b]*Department of Chemistry, Federal University of São Carlos, São Carlos, SP, Brazil*

[c]*Department of Physics and Astronomy, University of Alabama, Tuscaloosa, Alabama, USA. E-mail: paulo.t.araujo@ua.edu*

[d]*Institute of Natural Sciences, Graduate Program in Physics, Federal University of Pará, Belém, PA, Brazil. E-mail: barbosaneto@ufpa.br*

2. Materials and methods

2.1 Samples and spectroscopic measurements

The synthesis of **H_2TPyP** and its supramolecular **H_2TPyP [RuCl(dppb)(5,5′-Me-bipy)]$_4$** structure (**Supra-H_2TPyP**, see Fig. 1) follows the procedures described in the literature.[47,57] The

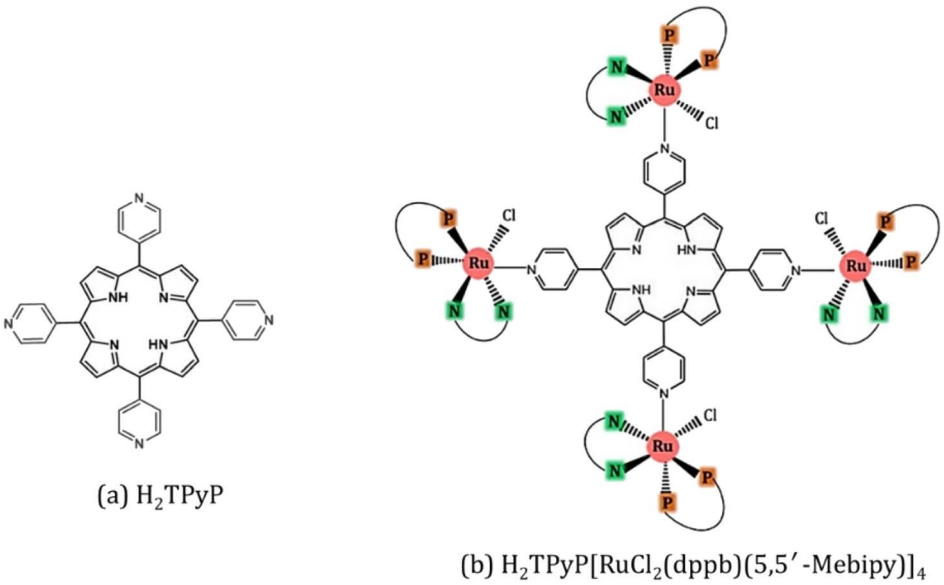

Fig. 1 (a) H_2TPyP and (b) **Supra-H_2TPyP**, with **$RuCl_2$(dppb)(5,5′-Mebipy)** ruthenium complexes attached at each (4-pyridyl) site of **H_2TPyP**. Here, 5,5′-Mebipy stands for 5,5′-dimethyl-2,2′-bipyridine (N–N), and dppb stands for 1,4-bis(diphenylphosphine) butane (P–P).

spectroscopic measurements were conducted with samples dissolved in $CHCl_3$ stabilized with amylene (NEON Inc.) used as received. Solution concentrations were kept below 10.0 μM to prevent spontaneous aggregation and inner filter effects. Absorption spectra were acquired with a JASCO V-670 spectrophotometer whereas steady-state photoluminescence (PL) spectra were measured using a setup composed of a Xenon lamp (ACTON); a monochromator (ACTON, model 300i) and a portable spectrophotometer (Ocean Optics), with the PL signal being detected in a 90° geometry relative to the excitation beam direction. Time-resolved PL experiments were conducted using a Time-Correlated Single Photon Counting (TCSPC) system (Horiba, Delta-Flex model with 27 ps of temporal resolution), equipped with a pulsed excitation source ($\lambda_{exc} = 352$ nm with 8.0 MHZ of repetition rate). The PL decays were collected at the maximum of each spectrum. Emission quantum yields[58,59] were calculated adopting **H_2TPyP** dissolved in $CHCl_3$ as standard[22] and applying eqn (1):

$$\Phi_{sa} = \Phi_{st} \frac{Abs_{st}}{Abs_{sa}} \frac{F_{sa}}{F_{st}}, \quad (1)$$

where, Φ_{sa} and Φ_{st} stand for the quantum yields of the sample (sa) and standard (st) solution, respectively. The quantities Abs_{st} (F_{st}) and Abs_{sa} (F_{sa}) are the absorbances at 420 nm (the integrated PL spectrum for the corresponding excitation) from the sample and standard solutions.

2.2. Photochemistry assays

For OPA in porphyrins, two sources (purchased from Laserline Inc), **green-OPA** (532 nm; ~4.0 W cm^{-2}, 19 200 J cm^{-2} total incident fluence, 90.0 minutes of irradiation) and **red-OPA** (635 nm; ~5.0 W cm^{-2}, 30 000 J cm^{-2} total incident fluence, 90.0 minutes of irradiation) were utilized. Here, ESA is promoted by a frequency-doubled Q-switched Nd-YAG laser (Quantel, model Q-smart 100, 6.0 ns FWHM, 532 nm excitation, 20.0 Hz of repetition rate, total incident fluence regime of ~2500 J cm^{-2}). The quantitative analysis of all irradiation conditions was performed by considering the effectively absorbed fluence instead of incident fluence. The relation between incident (F_I), transmitted (F_T) and absorbed (F_A) fluences is written as $F_I = F_T + F_A$, or $1 - \frac{F_T}{F_I} = \frac{F_A}{F_I}$.[58] From the Lambert–Beer law,[58] $\frac{F_T}{F_I} = 10^{-A(\lambda)}$ (with $A(\lambda)$ corresponding to absorbance at the incident wavelength, for the non-irradiated solution) resulting in eqn (2):

$$F_A = F_I(1 - 10^{-A(\lambda)}) \quad (2)$$

During all the spectroscopic measurements and irradiation processes, the samples were placed in sealed quartz cuvettes of 1.0 cm path length with four polished windows.

Control samples of **H_2TPyP** and **Supra-H_2TPyP** dissolved in $CHCl_3$ were kept in a dark environment at room temperature (~22.5 °C) to evaluate their stability. Absorption spectra confirm that no spontaneous modifications occur in both samples for 240.0 minutes of storage, endorsing their stability. This implies their durability is at least three times greater than the time demanded to perform the photo-induced reactions discussed herein.

3. Results and discussions

3.1 Photophysics of Supra-H_2TPyP

As shown in Fig. 2, the absorption spectrum of **Supra-H_2TPyP** displays red-shifted B- and Q-bands relative to **H_2TPyP**, in agreement with literature.[16,60] Additionally, signatures belonging to the metallic complex are also observed (see intra-ligand bands located at around 311 nm).[47,61–65] Due to their

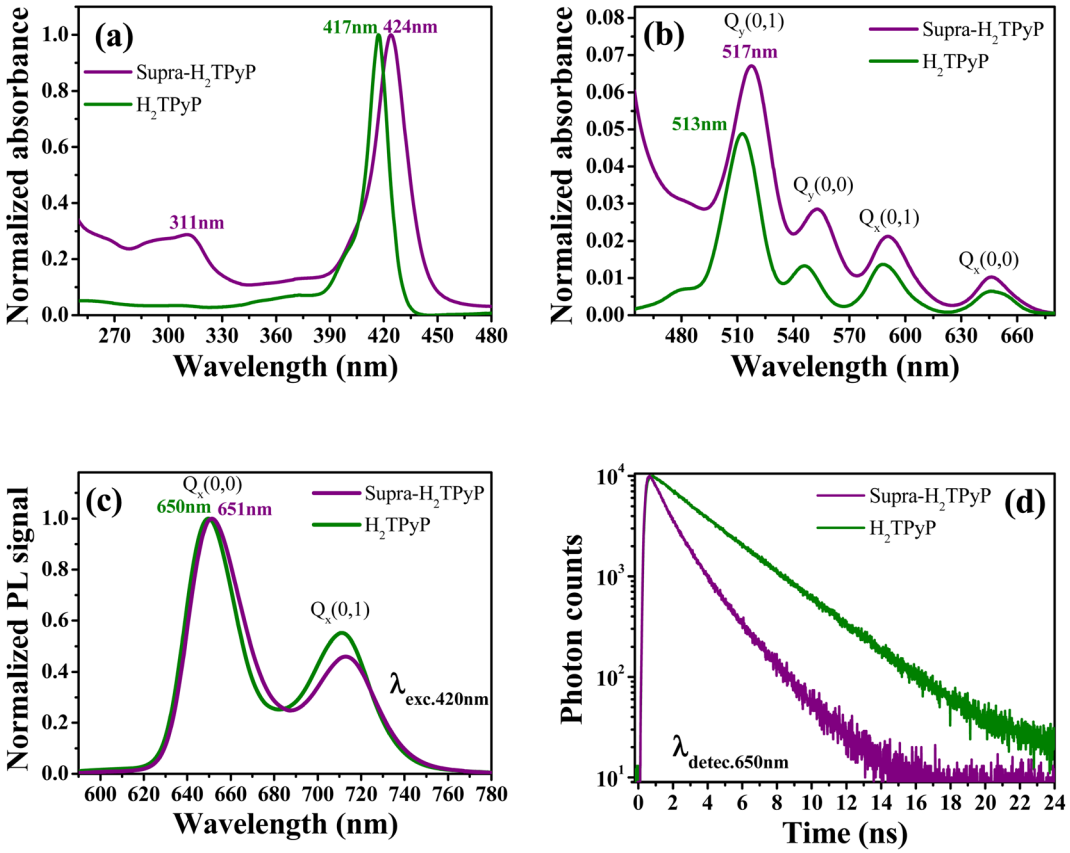

Fig. 2 Normalized absorption spectrum at (a) B- and (b) Q-bands. (c) Normalized PL spectrum ($\lambda_{exc.}$ = 420 nm) and (d) fluorescence decays ($\lambda_{detec.}$ = 650 nm) for H_2TPyP (green curves) and Supra-H_2TPyP (purple curves).

superposition with **H_2TPyP** bands, spectral signatures associated with the complex's MLCT bands centered around 470 nm are not resolved but lead to an overall increase of the spectrum baseline[49,52,56] (Fig. 2b).

The **Supra-H_2TPyP** PL spectrum (Fig. 2c) shows a small redshift (~1 nm) regarding **H_2TPyP**. This effect is accompanied by obtaining a 72% lower emission quantum yield for **Supra-H_2TPyP** concerning **H_2TPyP**[22] (see Table 1), in agreement with previous reports.[49–52] The **Supra-H_2TPyP** also presents a variation in the relative intensity between electronic (Q(0,0)) and vibronic (Q(0,1)) emission bands with relation to **H_2TPyP**, which indicates that either (1) the involved **H_2TPyP** vibronic progressions are changing[52,53] or (2) a new band arises and overlaps with **H_2TPyP** original bands.[52,53] From TCSPC experiments it is observed that the mono-exponential decay (7.26 ns) exhibited by **H_2TPyP** in $CHCl_3$[60] evolves to a bi-exponential decay (τ_1 = 2.01 ns (54%) and τ_2 = 4.54 ns (46%)) in **Supra-H_2TPyP** (Fig. 2d and Table 1). Based on the literature,[49,52,53] and considering that isolated ruthenium complexes do not exhibit emission bands around the probed wavelength (650 nm), τ_1 is associated with **Supra-H_2TPyP**, while the lifetime τ_2 is associated with the perturbed **H_2TPyP** deactivation pathway.[49,52,53] This trend supports the hypothesis of a novel band in the steady-state PL spectrum[53] (Fig. 2c).

3.2 Green-OPA irradiation of Supra-H_2TPyP

In chloroform, **H_2TPyP** is photostable under **green-OPA** irradiation.[15,16] This is not true for **Supra-H_2TPyP** under the same irradiation condition. Fig. 3 shows that the spectroscopic signatures of **Supra-H_2TPyP** are significantly modified as a function of the incident fluence. Because the modifications occur in different stages, the results are separately discussed in three fluence ranges: **(i)** 0–2400 J cm^2; **(ii)** 2400–6000 J cm^2; and **(iii)** 6000–19 200 J cm^{-2}.

Table 1 Photophysical features of H_2TPyP and Supra-H_2TPyP, dissolved in $CHCl_3$. Here, τ_2 (τ_1) refers to the excited state lifetime of the former (newly-formed) relaxation pathway

	B_{max} (nm)	Q_{max} (nm)	PL_{max} (nm)	τ_1 (ns)	τ_2 (ns)	Φ ($\times 10^{-2}$)
H_2TPyP	417	513	650	—	7.26 (100%)	1.61
Supra-H_2TPyP	424	517	651	2.01 (54%)	4.54 (46%)	0.45

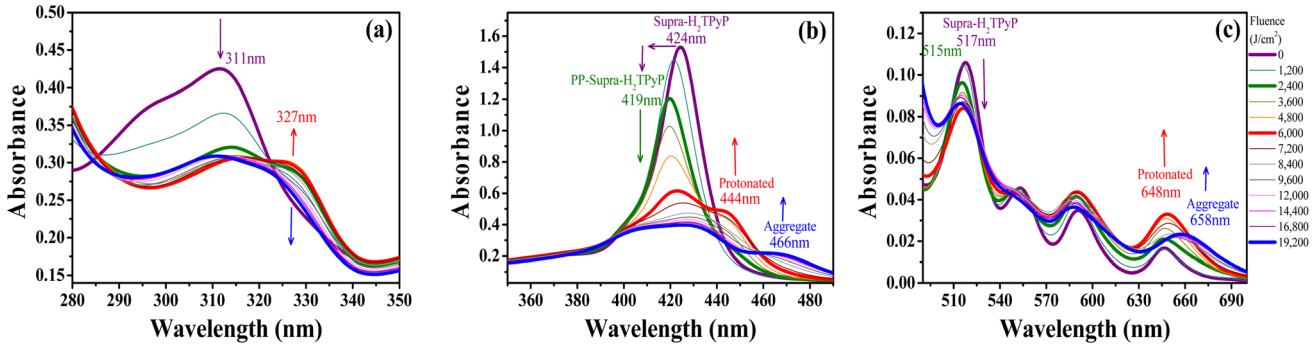

Fig. 3 Evolution of the absorption spectrum of **Supra-H_2TPyP** under **green-OPA** excitation (532 nm, 0–19200 J cm^{-2}) at (a) the UV bands (from 280 nm to 350 nm), (b) the B-band, and (c) the Q-band.

In range **(i)**, both B- and Q-bands undergo a blue shift. The main **Supra-H_2TPyP** B-band, originally centered at 424 nm (0 J cm^{-2}) (purple solid line), downshifts to 419 nm at 2400 J cm^{-2} (olive solid line) while the $Q_y(0,1)$ downshifts from 517 nm to 515 nm. This behavior suggests that **Supra-H_2TPyP** is undergoing a similar photodissociation as reported for the H_2TPyP $[RuCl_2(CO)(PPh_3)_2]_4$ tetraruthenated porphyrin.[53] The occurrence of photodissociation in the fluence range **(i)** would imply: (1) the decomposition of ruthenium complexes; and (2) the absence of processes associated with the fluence ranges **(ii)** and **(iii)**.[15,16] However, our data show that (1) and (2) do not happen, see Fig. 3. It is seen that in the fluence range **(i)**, the **RuCl(dppb)(5,5′-Me-bipy)** complexes in **Supra-H_2TPyP**, with intraligand bands spanning from ~280–360 nm, undergo a sort of transformation, forming a novel supramolecular species, baptized **PP-Supra-H_2TPyP**. The determination of the type of transformation that is photomodifying **RuCl(dppb)(5,5′-Me-bipy)** is out of the scope of this work but we understand that photooxidation,[66,67] photoisomerization,[68–70] and photoinduced ligand loss[71,72] are possible processes driving the phenomenon.

In range **(ii)**, the peak at 419 nm no longer blueshifts and starts developing into a novel spectroscopic signature centered at 444 nm, see Fig. 3b. The rise of this new signature occurs simultaneously with the enhancement of the $Q_x(0,0)$-band (around 648 nm). These are signatures associated with photoprotonation of **PP-Supra-H_2TPyP**.[15,16,73–75] Moreover, the **PP-Supra-H_2TPyP** 419 nm peak redshifts in ≈2 nm, which is a signature for the protonation of the photomodified **RuCl(dppb)(5,5′-Me-bipy)**.[16,76] In fact, a closer inspection of **RuCl(dppb)(5,5′-Me-bipy)** intraligand bands shows that the peak at ~327 nm is enhanced (Fig. 3a). It is important to recall that protonation requires acid environments. This is reported for complexes similar to **RuCl(dppb)(5,5′-Me-bipy)**, in which an acidic solution was created through the addition of aliquots of HCl.[77,78] Since we do not add any acid to our solutions, the observation of protonation of both the porphyrin and the photomodified **RuCl(dppb)(5,5′-Me-bipy)** confirms the release of HCl in the solution as a consequence of $CHCl_3$ photodecomposition *via* **green-OPA**.

In the range **(iii)**, it is observed that protonated **PP-Supra-H_2TPyP** signatures, B-(≈444 nm) and $Q_x(0,0)$-(≈648 nm) bands, disappear, which is followed by the rise of new bands at ≈466 nm and ≈658 nm, respectively. The new features indicate that the protonated **PP-Supra-H_2TPyP** is forming aggregates (possibly J-aggregates), similar to those previously reported for **H_2TPyP** under ESA excitation.[16] It is also observed that the intraligand band of the photomodified **RuCl(dppb)(5,5′-Me-bipy)** at 327 nm undergoes a decrease in intensity with no indications of further transformations.

The protonation of **Supra-H_2TPyP** also induces new signatures in the steady-state PL spectrum, which are in agreement with the results discussed above for UV-Vis absorption. Fig. 4a shows that the **Supra-H_2TPyP** PL spectrum (purple solid line) evolves to the protonated PL spectrum (red solid line).[16] After protonation, the PL signal continuously decreases with increasing fluence, becoming almost null at 19 200 J cm^{-2}. This decrease in the PL magnitude is associated with a reduction in the emission quantum yield of the protonated species, which is characteristic of J-aggregation in range **(iii)**.[16,74,79–83]

Fig. 4b shows that the **Supra-H_2TPyP** PL decay at 0 J cm^{-2} (purple solid line), which initially displays two characteristic lifetimes (4.54 ns (46%) and 2.01 ns (54%)), continuously evolves into the **PP-Supra-H_2TPyP** decay profile at 2400 J cm^{-2}, with a dominant characteristic lifetime of ≈7.01 ns (91%). A minor contributing lifetime of ≈ 3.17 ns (4%) is also measured and understood to belong to the remaining **Supra-H_2TPyP**. In addition, a new PL decay with a characteristic lifetime of 0.98 ns (5%) associated with the protonated **PP-Supra-H_2TPyP** is observed, see Table 2. The results in Fig. 4c and Table 2 support that in the range **(i)** both **Supra-H_2TPyP** and **PP-Supra-H_2TPyP** coexist. When the range (ii) starts (2400 J cm^{-2}), **PP-Supra-H_2TPyP** becomes predominant, coexisting with both **Supra-H_2TPyP** and the protonated **PP-Supra-H_2TPyP**. From 3600 J cm^{-2} on, the percentage contribution of the lifetime associated with **Supra-H_2TPyP** becomes negligible.

At 7200 J cm^{-2}, the **PP-Supra-H_2TPyP** (protonated **PP-Supra-H_2TPyP**) lifetime decreases from 7.01 ns (0.98 ns) to 6.84 ns (0.66 ns). Fig. 4d shows that, at 7200 J cm^{-2}, the quenching of these lifetimes, $\tau_{2(0)}/\tau_2$ (**PP-Supra-H_2TPyP**) and $\tau_{3(0)}/\tau_3$ (protonated **PP-Supra-H_2TPyP**), are 1.02 and 1.47, which originates from exciplex formation.[22] The quenching of the protonated **PP-Supra-H_2TPyP** is 144% more effective in comparison with that for **PP-Supra-H_2TPyP**. This result supports the presence of electrostatically-enhanced exciplex formed between the

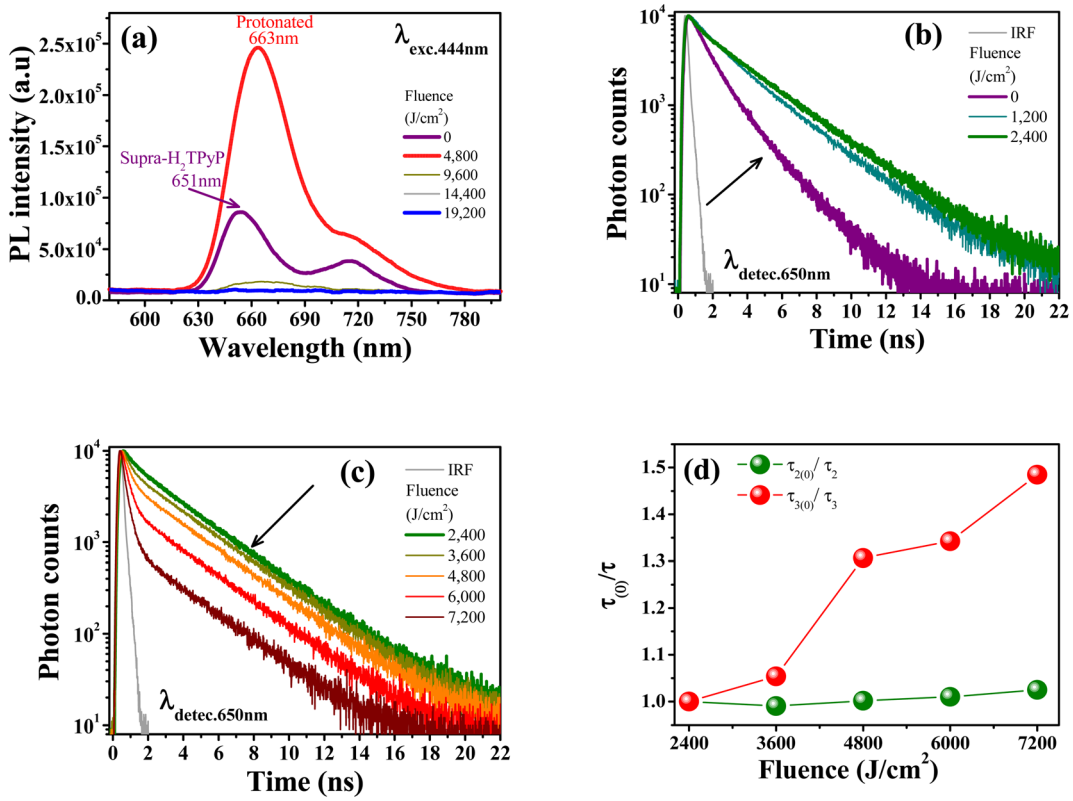

Fig. 4 (a) PL spectra evolution with increasing fluence ($\lambda_{exc.} = 444$ nm). **Supra-H_2TPyP** PL decay ($\lambda_{detec.} = 650$ nm) under **green-OPA** ($\lambda_{exc.} = 532$ nm) for: (b) fluence range **(i)**, and (c) fluence range **(ii)**. (d) Fluence dependence of the $\tau_{(0)}/\tau$ ratio for **PP-Supra-H_2TPyP** (green spheres) and its protonated counterpart (red spheres).

Table 2 Excited state decay parameters showing the evolution of **Supra-H_2TPyP** under **green-OPA**. The values in parentheses in the lifetime columns represent the percentage contribution of each fitting exponential. χ^2 estimates the fitting precision

Fluence (J cm^{-2})	τ_1 (ns)	τ_2 (ns)	τ_3 (ns)	χ^2
0	2.01 (54%)	4.54 (46%)	—	1.06
1200	2.16 (17%)	6.39 (83%)	—	1.03
2400	3.17 (4%)	7.01 (91%)	0.98 (5%)	1.07
3600		7.08 (89%)	0.93 (11%)	1.04
4800		7.00 (82%)	0.75 (18%)	1.06
6000		6.94 (65%)	0.73 (35%)	1.02
7200		6.84 (42%)	0.66 (58%)	1.12

positively charged protonated **PP-Supra-H_2TPyP** and Cl^- ions dispersed in the solution.[16] No discussion is addressed for range (iii) because the decrease in PL intensity invisibilized the PL decay measurements.

As discussed in the literature,[15,16] free base porphyrins (**H_2TPyP** and **H_2TPP**) under UV-OPA ($\lambda_{exc} = 266$ nm) and ESA ($\lambda_{exc} = 532$ nm) excitations are able to photodecompose $CHCl_3$ and form HCl with excitation energy thresholds located above the B-band energy ($\approx$2.97 eV).[15,16] This implies that these free-base porphyrins never underwent photoprotonation under **OPA** operating at 475 nm (2.61 eV) or 532 nm (2.33 eV).[15,16] In this work, we were able to photoprotonate **PP-Supra-H_2TPyP** dissolved in **$CHCl_3$** under **green-OPA** ($\approx$2.33 eV), meaning HCl is being formed as a consequence of **$CHCl_3$** decomposition. This process should not happen if the ground and the excited states of **PP-Supra-H_2TPyP** were similar in energy to the ground and the excited states of **H_2TPyP**. Since the excitation gap is fixed by the CW laser energy employed in **green-OPA** ($\approx$2.33 eV), our results indicate two possible scenarios: (1) the involved ground state in **PP-Supra-H_2TPyP** must be higher in energy in comparison to the correspondent state in **H_2TPyP** and/or (2) the photooxidative excited state in **PP-Supra-H_2TPyP** must be lower in energy concerning **H_2TPyP**.

3.3 Other irradiation conditions

Fig. 5a and b show the same photo-induced modifications (**PP-Supra-H_2TPyP** formation, photo-protonation, and photo-aggregation) in the spectroscopic signatures of **Supra-H_2TPyP** for **green-ESA** and **red-OPA** irradiations, respectively. The successful decomposition of **$CHCl_3$** under **red-OPA** irradiation (photon energy delivered $\approx$1.96 eV) sets a new lower limit for the excitation energy required to trigger the process.

To understand the photodecomposition rates under the different laser irradiation conditions, the **Supra-H_2TPyP** B-band integrated area (from 360 to 490 nm) for each laser absorbed fluence (F_A) was normalized by the B-band integrated area (also from 360 to 490 nm) of the reference non-irradiated **Supra-H_2TPyP**, and plotted as a function of F_A (see Fig. 6). The

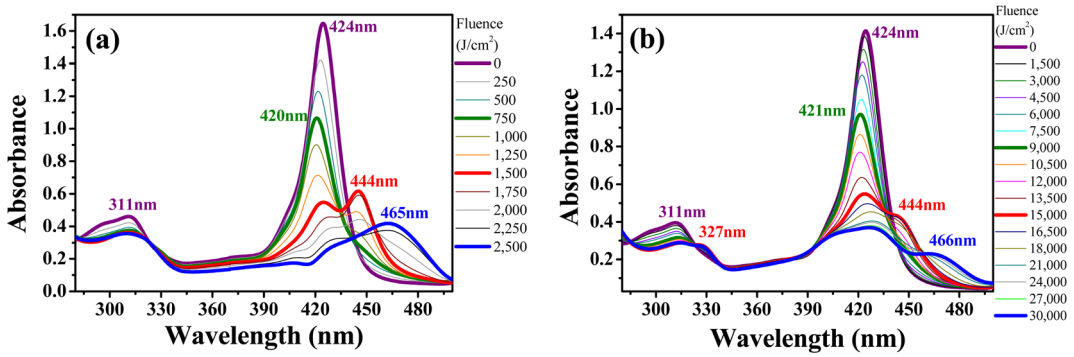

Fig. 5 Evolution of the absorption spectrum of **Supra-H_2TPyP** dissolved in $CHCl_3$ and irradiated under (a) **green-ESA** (532 nm, 6 ns, 0–2500 J cm^{-2}) and (b) **red-OPA** (633 nm, 0–19 200 J cm^{-2}).

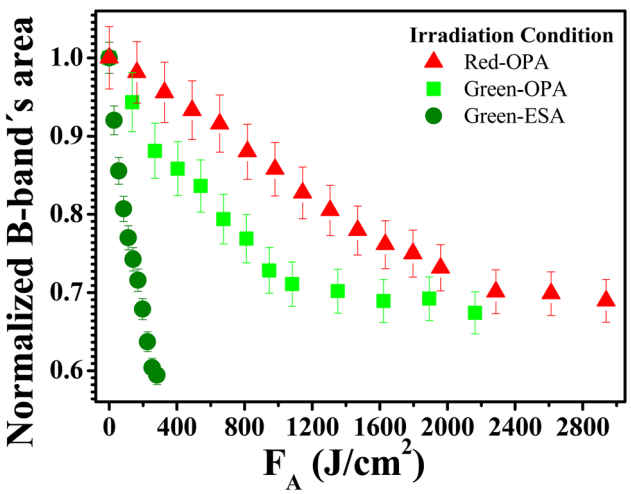

Fig. 6 Absorbed fluence-dependent evolutions of normalized B band's area comparing **green-ESA** (filled olive spheres), **green-OPA** (filled light-green circles), and **red-OPA** (filled red triangles) excitations applied to **Supra-H_2TPyP**.

exponential profiles obtained under each laser irradiation condition were fitted using $A_F = e^{(-kF_A)}$, where A_F and k represent, respectively, the aforementioned normalized areas for each F_A and the net photomodification rate (given in $cm^2\ J^{-1}$). The fitting results show that the rates obey the following hierarchy: **green-ESA** ($k = 4.32 \times 10^{-3}\ cm^2\ J^{-1}$) > **green-OPA** ($k = 1.43 \times 10^{-3}\ cm^2\ J^{-1}$) > **red-OPA** ($k = 0.50 \times 10^{-3}\ cm^2\ J^{-1}$), which shows that **green-ESA** leads to more efficient photoreaction processes in comparison with the **OPA**-based irradiations.

4. Conclusions

Supra-H_2TPyP places itself as an excellent candidate for a broad-range **OPA**-visible-light active molecular photocatalyst in dye-mediated chloroform decomposition. This supramolecular structure displays good photoreaction rates under visible **OPA** irradiation, which is a simpler and more affordable excitation mechanism than visible **ESA** and **UV-OPA.** Our results show that **Supra-H_2TPyP** when combined with different excitation wavelengths can be used to controllably photodecompose **$CHCl_3$** and, consequently, controllably photoprotonate **Supra-H_2TPyP** itself, which is also interesting for sensing chloroform in solution and other applications in fields like materials science.

Author contributions

J. M. S. Lopes: data curation, writing-original draft, writing – review & editing, investigation, visualization, formal analysis, methodology. A. A. Batista: writing-review & editing, data curation, formal Analysis, project administration, resources, validation. P. T. Araujo: data curation, writing-original draft, writing – review & editing, visualization, investigation, fund acquisition, supervision, project administration, validation, formal analysis, methodology. N. M. Barbosa Neto: data curation, writing – original draft, writing – review & editing, visualization, investigation, validation, formal analysis, methodology, supervision, resources, funding acquisition, project administration.

Conflicts of interest

The authors declare that they have no known competing financial interests or personal relationships that could have appeared to influence the work reported in this manuscript.

Acknowledgements

The Brazilian authors are indebted to the Brazilian National Council for Scientific and Technological Development (CNPq – processes numbers: 306147/2020-3 and 425124/2018-5), São Paulo Research Foundation (FAPESP – process number: 2014/50869-6) and the Education Ministry (CAPES – Process number: 23038.000776/201754) *via* the projects of the National Institute for Science and Technology on Organic Electronics and with Amazonian Foundation for the Support of Studies and Research (FAPESPA – process number: 88881.159129/2017-01). N. M. B. N. is especially indebted to the Fulbright Foundation for its Visiting Professor Award Grant. P. T. A. acknowledges the National Science Foundation for supporting this work under the CAREER grant # CHE-1848418. The authors are also grateful to Prof. Sanclayton Moreira, of the Graduate Program in

Physics of the Federal University of Para, for granting access to his experimental facilities.

References

1 C. Hang, B. Zhang, T. Gong and Q. Xian, Occurrence and health risk assessment of halogenated disinfection byproducts in indoor swimming pool water, *Sci. Total Environ.*, 2016, **543**, 425–431.
2 S. Chowdhury, K. Al-hooshani and T. Karanfil, Disinfection byproducts in swimming pool: occurrences, implications and future needs, *Water Res.*, 2014, **53**, 68–109.
3 H. Kim, J. Shim and S. Lee, Formation of disinfection by-products in chlorinated swimming pool water, *Chemosphere*, 2002, **46**, 123–130.
4 J. Lee, M. J. Jun, M. H. Lee, M. H. Lee, S. W. Eom and K. D. Zoh, Production of various disinfection byproducts in indoor swimming pool waters treated with different disinfection methods, *Int. J. Hyg. Environ. Health*, 2010, **213**, 465–474.
5 M. Panyakapo, S. Soontornchai and P. Paopuree, Cancer risk assessment from exposure to trihalomethanes in tap water and swimming pool water, *J. Environ. Sci.*, 2008, **20**, 372–378.
6 L. O. Vajrabhaya, S. K. Suwannawong, R. Kamolroongwarakul and L. Pewklieng, Cytotoxicity evaluation of gutta-percha solvents: chloroform and GP-solvent (limonene), *Oral Surg. Oral Med. Oral Pathol. Oral Radiol. Endod.*, 2004, **98**, 756–759.
7 M. V Templin, K. C. Jamison, C. S. Sprankle, D. C. Wolf, B. A. Wong and B. E. Butterworth, Chloroform-induced cytotoxicity and regenerative cell proliferation in the kidneys and liver of BDF1 mice, *Cancer Lett.*, 1996, **108**, 225–231.
8 J. F. Larson, D. C. Wolf and B. E. Butterworth, Induced cytotoxicity and cell proliferation in the hepatocarcinogenicity of chloroform in female b6c3f1 mice: comparison of administration by gavage in corn oil *vs.* ad Libitum in drinking water, *Fundam. Appl. Toxicol.*, 1994, **22**, 90–102.
9 M. Shariati-Rad and F. Fattahi, A simple equipment and colorimetric method for determination of chloroform in water, *Anal. Chim. Acta*, 2020, **1100**, 208–214.
10 V. Choudhary, K. Vellingiri and L. Philip, Potential nanomaterials-based detection and treatment methods for aqueous chloroform, *Environ. Nanotechnol., Monit. Manage.*, 2021, **16**, 100487.
11 K. Sheng, H. Lu, A. Sun, Y. Wang, Y. Liu, F. Chen, W. Bian, Y. Li, R. Kuang and D. Sun, A naked-eye colorimetric sensor for chloroform, *Chin. Chem. Lett.*, 2019, **30**, 895–898.
12 D. Fernández-Verdejo, P. Cortés, A. Guisasola, P. Blánquez and E. Marco-Urrea, Bioelectrochemically-assisted degradation of chloroform by a co-culture of Dehalobacter and Dehalobacterium, *Environ. Sci. Ecotechnology*, 2022, **12**, 5.
13 H. Wang, R. Yu, J. Webb, P. Dollar and D. L. Freedman, Anaerobic Biodegradation of Chloroform and Dichloromethane with a Dehalobacter Enrichment Culture, *Appl. Environ. Microbiol.*, 2022, **88**(4), e01970.
14 J. Jose, S. Ramanujam and L. Philip, Applicability of pulsed corona discharge treatment for the degradation of chloroform, *Chem. Eng. J.*, 2019, **360**, 1341–1354.
15 Z. Muñoz, A. S. Cohen, L. M. Nguyen, T. A. McIntosh and P. E. Hoggard, Photocatalysis by tetraphenylporphyrin of the decomposition of chloroform, *Photochem. Photobiol. Sci.*, 2008, **7**, 337–343.
16 J. M. S. Lopes, A. E. H. Machado, A. A. Batista, P. T. Araujo and N. M. Barbosa Neto, Protonation, exciplex, and evidence of aggregate formation in *meso*-tetra(4-pyridyl) porphyrin triggered by excited-state absorption, *J. Photochem. Photobiol., A*, 2022, **426**, 113759.
17 R. Gilbert, M. Karabulut and P. E. Hoggard, Photocatalysis of chloroform degradation by μ-dichlorotetrachlorodipalladate(II), *Inorg. Chim. Acta*, 2010, **363**, 1462–1468.
18 L. A. Peña and P. E. Hoggard, Hexachlororhodate(III) and the photocatalytic decomposition of chloroform, *J. Mol. Catal. A: Chem.*, 2010, **327**, 20–24.
19 L. A. Peña, A. J. Seidl, L. R. Cohen and P. E. Hoggard, Ferrocene/ferrocenium ion as a catalyst for the photodecomposition of chloroform, *Transition Met. Chem.*, 2009, **34**, 135–141.
20 A. J. Seidl, L. R. Cohen, L. A. Peña and P. E. Hoggard, Chlorochromate ion as a catalyst for the photodegradation of chloroform by visible light, *Photochem. Photobiol. Sci.*, 2008, **7**, 1373–1377.
21 D. Dolphin, The Porphyrins, Volume III. Physical Chemistry, Part A, *The Porphyrins*, 1978, vol. 3, p. 640.
22 J. M. S. Lopes, J. R. T. Reis, A. E. H. Machado, T. H. O. Leite, A. A. Batista, T. V. Acunha, B. A. Iglesias, P. T. Araujo and N. M. Barbosa Neto, Influence of the *meso*-substituents on the spectral features of free-base porphyrin, *Spectrochim. Acta, Part A*, 2020, **238**, 118389.
23 A. K. Mandal, M. Taniguchi, J. R. Diers, D. M. Niedzwiedzki, C. Kirmaier, J. S. Lindsey, D. F. Bocian and D. Holten, Photophysical properties and electronic structure of porphyrins bearing zero to four *meso*-phenyl substituents: new insights into seemingly well understood tetrapyrroles, *J. Phys. Chem. A*, 2016, **120**, 9719–9731.
24 J. S. Baskin, H. Z. Yu and A. H. Zewail, Ultrafast dynamics of porphyrins in the condensed phase: I. Free base tetraphenylporphyrin, *J. Phys. Chem. A*, 2002, **106**, 9837–9844.
25 H. Z. Yu, J. S. Baskin and A. H. Zewail, Ultrafast dynamics of porphyrins in the condensed phase: II. Zinc tetraphenylporphyrin, *J. Phys. Chem. A*, 2002, **106**, 9845–9854.
26 J. Jing, J. Yang, Z. Zhang and Y. Zhu, Supramolecular Zinc Porphyrin Photocatalyst with Strong Reduction Ability and Robust Built-In Electric Field for Highly Efficient Hydrogen Production, *Adv. Energy Mater.*, 2021, **11**, 1–7.
27 T. Shiragami, J. Matsumoto, H. Inoue and M. Yasuda, Antimony porphyrin complexes as visible-light driven photocatalyst, *J. Photochem. Photobiol., C*, 2005, **6**, 227–248.

28 Z. Zhang, Y. Zhu, X. Chen, H. Zhang and J. Wang, A Full-Spectrum Metal-Free Porphyrin Supramolecular Photocatalyst for Dual Functions of Highly Efficient Hydrogen and Oxygen Evolution, *Adv. Mater.*, 2019, **31**, 1–6.
29 Y. Chen, A. Li, Z. H. Huang, L. N. Wang and F. Kang, Porphyrin-based nanostructures for photocatalytic applications, *Nanomaterials*, 2016, **6**, 1–17.
30 M. K. Panda, K. Ladomenou and A. G. Coutsolelos, Porphyrins in bio-inspired transformations: light-harvesting to solar cell, *Coord. Chem. Rev.*, 2012, **256**, 2601–2627.
31 T. Higashino and H. Imahori, Porphyrins as excellent dyes for dye-sensitized solar cells: recent developments and insights, *Dalton Trans.*, 2015, **44**, 448–463.
32 L. L. Li and E. W. G. Diau, Porphyrin-sensitized solar cells, *Chem. Soc. Rev.*, 2013, **42**, 291–304.
33 S. Mathew, A. Yella, P. Gao, R. Humphry-Baker, B. F. E. Curchod, N. Ashari-Astani, I. Tavernelli, U. Rothlisberger, M. K. Nazeeruddin and M. Grätzel, Dye-sensitized solar cells with 13% efficiency achieved through the molecular engineering of porphyrin sensitizers, *Nat. Chem.*, 2014, **6**, 242–247.
34 M. Ethirajan, Y. Chen, P. Joshi and R. K. Pandey, The role of porphyrin chemistry in tumor imaging and photodynamic therapy, *Chem. Soc. Rev.*, 2011, **40**, 340–362.
35 A. E. O'Connor, W. M. Gallagher and A. T. Byrne, Porphyrin and nonporphyrin photosensitizers in oncology: preclinical and clinical advances in photodynamic therapy, *Photochem. Photobiol.*, 2009, **85**, 1053–1074.
36 J. Kou, D. Dou and L. Yang, Porphyrin photosensitizers in photodynamic therapy and its applications, *Oncotarget*, 2017, **8**, 81591–81603.
37 H. Imahori, Porphyrin – fullerene linked systems as artificial photosynthetic mimics, *Org. Biomol. Chem.*, 2004, (2), 1425–1433.
38 Y. Nakamura, N. Aratani and A. Osuka, Cyclic porphyrin arrays as artificial photosynthetic antenna: synthesis and excitation energy transfer, *Chem. Soc. Rev.*, 2007, **36**, 831–845.
39 N. Zarrabi and P. K. Poddutoori, Aluminum(III) porphyrin: a unique building block for artificial photosynthetic systems, *Coord. Chem. Rev.*, 2021, **429**, 213561.
40 N. M. Boyle, J. Rochford and M. T. Pryce, Thienyl-Appended porphyrins: synthesis, photophysical and electrochemical properties, and their applications, *Coord. Chem. Rev.*, 2010, **254**, 77–102.
41 J. M. S. Lopes, R. N. Sampaio, A. S. Ito, A. A. Batista, A. E. H. Machado, P. T. Araujo and N. M. B. Neto, Evolution of electronic and vibronic transitions in metal(II) *meso*-tetra(4-pyridyl)porphyrins, *Spectrochim. Acta, Part A*, 2019, **215**, 327–333.
42 F. Hajjaj, Z. S. Yoon, M. C. Yoon, J. Park, A. Satake, D. Kim and Y. Kobuke, Assemblies of supramolecular porphyrin dimers in pentagonal and hexagonal arrays exhibiting light-harvesting antenna function, *J. Am. Chem. Soc.*, 2006, **128**, 4612–4623.
43 T. Tanaka and A. Osuka, Conjugated porphyrin arrays: synthesis, properties and applications for functional materials, *Chem. Soc. Rev.*, 2015, **44**, 943–969.
44 E. Alessio, E. Ciani, E. Iengo, V. Y. Kukushkin and L. G. Marzilli, Stepwise assembly of unsymmetrical supramolecular arrays containing porphyrins and coordination compounds, *Inorg. Chem.*, 2000, **39**, 1434–1443.
45 H. E. Toma and K. Araki, Supramolecular assemblies of ruthenium complexes and porphyrins, *Coord. Chem. Rev.*, 2000, **196**, 307–329.
46 H. E. Toma and K. Araki, Exploring the supramolecular coordination chemistry-based approach for nanotechnology, *Prog. Inorg. Chem.*, 2009, **56**, 379–485.
47 T. H. O. Leite, G. Grawe, J. Honorato, B. N. Cunha, O. R. Nascimento, P. S. De Vargas, C. Donatoni, K. T. Oliveira, J. M. S. Lopes, N. M. Barbosa Neto, W. C. Moreira, L. R. Dinelli and A. A. Batista, Remarkable Electronic Effect on the *meso*-Tetra(thienyl)porphyrins, *Inorg. Chem.*, 2019, **58**, 1030–1039.
48 N. M. B. Neto, S. L. Oliveira, I. Guedes, L. R. Dinelli and L. Misoguti, Reverse Saturable Absorption in 5,10,15,20-Tetra(4-pyridyl)-21*H*,23*H*-porphyrin with Ruthenium Outlying Complexes, *J. Braz. Chem. Soc.*, 2006, **17**(7), 1377–1382.
49 R. N. Sampaio, M. M. Silva, A. A. Batista and N. M. B. Neto, Investigation of the photophysical and electrochemical properties of a free base tetrapyridyl porphyrin with *meso* carbon linked ruthenium(II) groups, *J. Photochem. Photobiol., A*, 2016, **315**, 98–106.
50 A. Prodi, M. Teresa, C. J. Kle and E. Alessio, Energy transfer pathways in pyridylporphyrin metal adducts and side-to-face arrays, *Coord. Chem. Rev.*, 2002, **229**(1–2), 51–58.
51 A. Prodi, C. J. Kleverlaan, M. T. Indelli, F. Scandola, D. Chimica, E. Alessio, E. Iengo, S. Chimiche and R. V January, Photophysics of Pyridylporphyrin Ru(II) Adducts: Heavy-Atom Effects and Intramolecular Decay Pathways, *Inorg. Chem.*, 2001, **40**(14), 3498–3504.
52 R. N. Sampaio, W. R. Gomes, D. M. S. Araujo, A. E. H. Machado, R. A. Silva, A. Marletta, I. E. Borissevitch, A. S. Ito, L. R. Dinelli, A. A. Batista, S. C. Zílio, P. J. Gonçalves and N. M. Barbosa Neto, Investigation of Ground- and Excited-State Photophysical Properties Outlying Complexes, *J. Phys. Chem. A*, 2012, **116**, 18–26.
53 J. M. S. Lopes, S. N. Costa, A. A. Batista, L. R. Dinelli, P. T. Araujo and N. M. B. Neto, Photophysics and visible light photodissociation of supramolecular *meso*-tetra(4-pyridyl) porphyrin/$RuCl_2(CO)(PPh_3)_2$ structures, *Spectrochim. Acta, Part A*, 2020, **237**, 118351.
54 J. M. S. Lopes, R. N. Sampaio, L. R. Dinelli, A. A. Batista, P. T. Araujo and N. M. B. Neto, On the excitation dependence of fluorescence spectra of *meso*-tetrapyridyl zinc(II) porphyrin and its relation with hydrogen bonding and outlying decoration, *Spectrochim. Acta, Part A*, 2020, **224**, 117371.

55 J. M. S. Lopes, S. N. Costa, E. Silveira-Alves Jr, A. A. Batista, P. J. Gonçalves, L. R. Dinelli, P. T. Araujo and N. M. Barbosa Neto, Singlet Oxygen Generation and Spectroscopic Properties of Supramolecular Zinc *Meso*–tetra (4-pyridyl) Porphyrin Bearing Outlying Ruthenium Groups, *Braz. J. Phys.*, 2022, 38–40.

56 M. I. F. Barbosa, G. G. Parra, R. S. Correa, R. N. Sampaio, L. N. Magno, R. C. Silva, A. C. Doriguetto, J. Ellena, N. M. B. Neto, A. A. Batista and P. J. Gonçalves, Reactive nitrogen/oxygen species production by nitro/nitrosyl supramolecular ruthenium porphyrin complexes, *J. Photochem. Photobiol., A*, 2017, **338**, 152–160.

57 N. M. Barbosa Neto, L. De Boni, J. J. Rodrigues Jr, L. Misoguti, C. R. Mendonça, L. R. Dinelli, A. A. Batista and S. C. Zilio, Dynamic saturable optical nonlinearities in free base porphyrins, *J. Porphyr. Phthalocyanines*, 2003, **7**, 452–456.

58 B. Valeur and M. N. Berberan-Santos, *Molecular Fluorescence: Principles and Applications*, Wiley-VCH Verlag & Co, Weinheim, 2nd edn, 2012.

59 J. R. Lakowicz, *Principles of Fluorescence Spectroscopy*, Springer, New York, 3rd edn, 2006.

60 J. M. S. Lopes, K. Sharma, R. N. Sampaio, A. A. Batista, A. S. Ito, A. E. H. Machado, P. T. Araújo and N. M. Barbosa Neto, Novel insights on the vibronic transitions in free base *meso*-tetrapyridyl porphyrin, *Spectrochim. Acta, Part A*, 2019, **209**, 274–279.

61 R. M. O'Donnell, P. G. Johansson, M. Abrahamsson and G. J. Meyer, Excited-state relaxation of ruthenium polypyridyl compounds relevant to dye-sensitized solar cells, *Inorg. Chem.*, 2013, **52**, 8282.

62 D. S. Seneviratne, M. J. Uddin, V. Swayambunathan, H. B. Schlegel and J. F. Endicott, Characteristics and properties of metal-to-ligand charge-transfer excited states in 2,3-bis(2-pyridyl)pyrazine and 2,2′-bipyridine ruthenium complexes. Perturbation-theory-based correlations of optical absorption and emission parameters with electrochemis, *Inorg. Chem.*, 2002, **41**, 1502–1517.

63 D. W. Thompson, A. Ito and T. J. Meyer, [Ru(bpy)3]2+* and other remarkable metal-to-ligand charge transfer (MLCT) excited states, *Pure Appl. Chem.*, 2013, **85**, 1257–1305.

64 X. Y. Wang, A. Del Guerzo and R. H. Schmehl, Photophysical behavior of transition metal complexes having interacting ligand localized and metal-to-ligand charge transfer states, *J. Photochem. Photobiol., C*, 2004, **5**, 55–77.

65 X. Han, L. Z. Wu, G. Si, J. Pan, Q. Z. Yang, L. P. Zhang and C. H. Tung, Switching between ligand-to-ligand charge-transfer, intraligand charge-transfer, and metal-to-ligand charge-transfer excited states in platinum(II) terpyridyl acetylide complexes induced by pH change and metal ions, *Chem.–Eur. J.*, 2007, **13**, 1231–1239.

66 A. Ülveczky and A. Horváth, Photooxidation of Ru (bpy) $(CN)_4^{2-}$ and Ru (DMbpy) $(CN)_4^{2-}$, *Inorg. Chim. Acta*, 1995, **236**, 173–176.

67 Z. Z. Li, Y. L. Niu, H. Y. Zhou, H. Y. Chao and B. H. Ye, Visible-light-induced photooxidation of ruthenium(II) complex with 2,2′-biimidazole-like ligand by singlet oxygen, *Inorg. Chem.*, 2013, **52**, 10087–10095.

68 R. Girotti, A. Romerosa, S. Mañas, S. R. Manuel and R. N. Perutz, Visible-light photoisomerization and photoaquation of trans-[Ru(1,3,5-triaza-7-phosphaadamantane)$_4$Cl$_2$] in organic solvent and water, *Inorg. Chem.*, 2009, **48**, 3692–3698.

69 S. J. Wezenberg, K. Y. Chen and B. L. Feringa, Visible-Light-Driven Photoisomerization and Increased Rotation Speed of a Molecular Motor Acting as a Ligand in a Ruthenium(II) Complex, *Angew. Chem., Int. Ed.*, 2015, **54**, 11457–11461.

70 M. O. Santiago, C. L. Donicci Filho, I. de S. Moreira, R. M. Carlos, S. L. Queiroz and A. A. Batista, Photochemical isomerization of trans- to cis-[RuCl2(dppb)(4,4′-X2-2,2′-bipy)] (X = –H, –NO_2, –Me, –COOH, –SMe, –O = SMe, –Cl, –OMe) complexes, *Polyhedron*, 2003, **22**, 3205–3211.

71 Z. J. Fuller, W. D. Bare, K. A. Kneas, W. Y. Xu, J. N. Demas and B. A. DeGraff, Photostability of luminescent ruthenium(II) complexes in polymers and in solution, *Anal. Chem.*, 2003, **75**, 2670–2677.

72 D. W. Thompson, C. N. Fleming, B. D. Myron and T. J. Meyer, Rigid medium stabilization of metal-to-ligand charge transfer excited states, *J. Phys. Chem. B*, 2007, **111**, 6930–6941.

73 J. R. Weinkauf, S. W. Cooper, A. Schweiger and C. C. Wamser, Substituent and solvent effects on the hyperporphyrin spectra of diprotonated tetraphenylporphyrins, *J. Phys. Chem. A*, 2003, **107**, 3486–3496.

74 M. Zannotti, R. Giovannetti, B. Minofar, D. Řeha, L. Plačková, C. A. D'Amato, E. Rommozzi, H. V. Dudko, N. Kari and M. Minicucci, Aggregation and metal-complexation behaviour of THPP porphyrin in ethanol/water solutions as function of pH, *Spectrochim. Acta, Part A*, 2018, **193**, 235–248.

75 I. Gupta and M. Ravikanth, Spectroscopic properties of *meso*-thienylporphyrins with different porphyrin cores, *J. Photochem. Photobiol., A*, 2006, **177**, 156–163.

76 Y. Fang, J. Zhu, Y. Cui, L. Zeng, M. L. Naitana, Y. Chang, N. Desbois, C. P. Gros and K. M. Kadish, Protonation and Electrochemical Properties of Pyridyl- and Sulfonatophenyl-Substituted Porphyrins in Nonaqueous Media, *ChemElectroChem*, 2017, **4**, 1872–1884.

77 P. A. Anderson, R. F. Anderson, M. Furue, P. C. Junk, F. R. Keene, B. T. Patterson and B. D. Yeomans, Protonation studies of reduced ruthenium(II) complexes with polypyridyl ligands, *Inorg. Chem.*, 2000, **39**, 2721–2728.

78 S. Zhang and R. E. Shepherd, Protonation of coordinated 2-methylpyrazine and 4,4′-bipyridine as a probe of n-donor potential of ruthenium(II) polyaminopoly-carboxylate complexes, *Transition Met. Chem.*, 1992, **17**, 199–203.

79 J. Mosinger, M. Janošková, K. Lang and P. Kubát, Light-induced aggregation of cationic porphyrins, *J. Photochem. Photobiol., A*, 2006, **181**, 283–289.

80 N. C. Maiti, S. Mazumdar and N. Periasamy, J- and H-aggregates of porphyrin-surfactant complexes: time-

resolved fluorescence and other spectroscopic Studies, *J. Phys. Chem. B*, 1998, **102**, 1528–1538.

81 G. De Luca, A. Romeo and L. M. Scolaro, Role of counteranions in acid-induced aggregation of isomeric tetrapyridylporphyrins in organic solvents, *J. Phys. Chem. B*, 2005, **109**, 7149–7158.

82 Y. Arai and H. Segawa, Cl- complexation induced H- and J-Aggregates of *meso*-tetrakis-(4-sulfonatothienyl)porphyrin diacid in aqueous solution, *J. Phys. Chem. B*, 2011, **115**, 773–7780.

83 G. De Luca, A. Romeo and L. M. Scolaro, Aggregation properties of hyperporphyrins with hydroxyphenyl substituents, *J. Phys. Chem. B*, 2006, **110**, 14135–14141.